Mechanical Engineering Advances 2026, 4(1), 4365.
doi: https://doi.org/10.59400/mea4365

Article

Thermo-elastic stress and deformation analysis of optical filters satellites payload

Fatouma Maamar

Algerian Space Agency, Satellites Development Center, Oran 31130, Algeria; fmaamar@cds.asal.dz

CITATION

Maamar F. Thermo-elastic stress and deformation analysis of optical filters satellites payload. Mechanical Engineering Advances. 2026; 4(1): 4365.
https://doi.org/10.59400/mea4365

ARTICLE INFO

Received: 2 January 2026
Revised: 19 February 2026
Accepted: 23 February 2026
Available online: 4 March 2026

Abstract: Modern optical filter systems used in space applications are required to operate under severe thermal and mechanical environments for extended mission durations without degradation of their optical or structural performance. However, the deposition of multilayer onto optical substrates with different thermo-mechanical properties can generate residual and thermally induced stresses. These stresses may lead to substrate deformation, degradation of optical performance, and damage to the bonding interfaces between the optical filter and its supporting structure. In this study, a comprehensive thermo-elastic analysis of an optical filter assembly, including the coated substrate, adhesive glue pads, and filter tray, is carried out using the finite element method. A detailed three-dimensional numerical model was developed in ANSYS to investigate the thermo-mechanical response of the assembly under representative thermal loading conditions corresponding to the operational environment of a spaceborne optical payload. The analysis focuses on the evaluation of Von Mises stresses, thermal deformations, and the structural integrity of the adhesive bonding regions, which are considered critical areas for the reliability of the assembly. The primary objective of this work is to assess and validate the structural design of the optical filter tray implemented in the ALSAT-1B satellite payload and to quantify the effects of thermal loading on the mechanical behavior of the bonded optical components. The numerical results are further used to evaluate the structural margins and identify potential failure risks associated with thermal contraction and material mismatch effects. The results indicate that the configuration with a higher number of glue pad contact points between the optical filter and filter tray provides the most favorable mechanical behavior, significantly reducing the risk of on-orbit failure.

Keywords: optical filter design; assembly tray; glue pads; MOS (margin of safety); filter deformation

1. Introduction

Spaceborne optical payloads require highly stable optomechanical structures capable of maintaining optical alignment and imaging performance under severe mechanical and thermal environments encountered during launch and orbital operation. Earth observation satellites [1–5], such as Alsat-1B, rely on multispectral optical systems integrating focal plane assemblies (FPAs), CCD detectors, and optical filters to acquire high-resolution images in panchromatic and multispectral bands. The optical performance of these systems is strongly dependent on the dimensional stability of the optical components and their mounting interfaces.

The focal plane assembly generally includes several spectral filters corresponding to the blue, green, red, near-infrared (NIR), and panchromatic (PAN) channels. These

filters are commonly bonded to the supporting tray using adhesive pads in order to ensure accurate positioning, reduced mass, vibration damping, and improved thermo-mechanical compatibility compared with conventional mechanical fastening techniques. However, adhesive bonding introduces complex thermo-mechanical interactions caused by differences in the coefficients of thermal expansion (CTE) between the filter substrate, adhesive layer, and supporting structure. These mismatches may generate thermo-elastic stresses, deformation, optical distortion, and alignment errors, particularly under cryogenic or non-operational temperature conditions [6–9].

Recent advances in thin-film coating technologies have enabled the development of increasingly complex optical filters with enhanced spectral characteristics and higher functional requirements. However, the deposition of multilayer thin-film coatings onto optical substrates having different thermo-mechanical properties can generate residual and thermally induced stresses [6, 10].

Several studies have investigated the behavior of bonded optical systems subjected to thermal and mechanical loading. Maamar et al. [11] demonstrated that glue-pad configurations strongly influence stress distribution and optical deformation in space optomechanical assemblies, and showed that six-point bonding configurations provide improved stability for optics mounting applications. Other researchers [12–14] have highlighted that thermo-elastic stresses generated by CTE mismatch can induce birefringence, optical path difference (OPD), and surface deformation, which directly affect imaging quality in high-resolution optical systems.

Finite element analysis (FEA) has become an essential tool for evaluating thermo-mechanical behavior in focal plane assemblies and bonded optical structures. Numerical simulations performed using commercial software such as ANSYS enable accurate prediction of stress concentration, displacement, deformation, and safety margins under combined thermal and inertial loading conditions. Previous investigations on infrared focal plane arrays and optomechanical lens assemblies demonstrated that thermo-elastic stresses increase significantly at low temperatures due to constrained thermal contraction and material incompatibility [15–19].

In addition to numerical analysis, analytical thermo-elastic models are frequently employed to estimate axial deformation and thermal strain in bonded optical systems. Comparisons between analytical predictions and finite element simulations generally show good agreement, validating the use of simplified thermo-elastic formulations during preliminary design stages [20–23]. Nevertheless, finite element models remain necessary to account for realistic assembly constraints, adhesive behavior, and local stress concentrations.

In this work, a thermo-mechanical investigation of the bonded optical filter assembly of the Alsat-1B payload is presented. The study focuses on the evaluation of thermo-elastic stresses, Margin of Safety (MOS), and axial deformation of the optical filters under thermal and inertial loading conditions representative of launch and qualification environments. The objective is to assess the structural integrity and dimensional stability of the adhesive-bonded filter assembly and to validate the suitability of the selected bonding configuration for space applications.

2. Materials and methods

2.1. Description of the payload design

The Algerian Earth observation satellite Alsat-1B has a total mass of 110 kg, including approximately 18.5 kg for the Alite payload (**Figure 1**), and was launched aboard the PSLV-C35 on 26 September 2016. The payload is designed to acquire raw image data in one panchromatic (PAN) band and four multispectral (MS) bands (blue, green, red, and near-infrared), while delivering digitized pixel data to the High-Speed Data Recorder (HSDR). The imaging system provides a spatial resolution of 12 m in PAN mode and 24 m in MS mode, with the capability of acquiring enhanced 12 m multispectral images. The payload architecture is based on an optical telescope composed of aluminum and titanium structural elements integrated with a set of nine optical lenses. It incorporates a low thermal-expansion focal plane assembly equipped with five linear CCD detectors coupled to spectral optical filters, which are slightly tilted to minimize stray-light effects and improve image quality. The payload is further supported by proximity Front-End Electronics (FEE) and instrument electronics that provide management functions and integrate the mass memory system (HSDR), as illustrated in **Figure 2**.

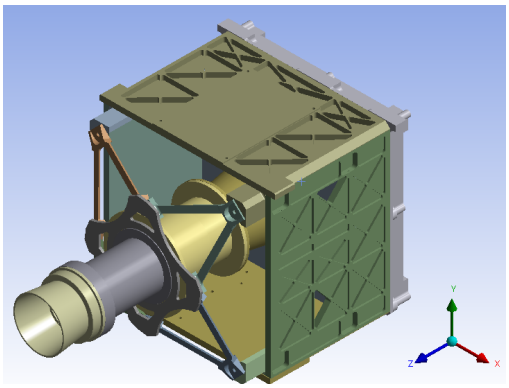

Figure 1. A CAD model of the camera assembly (Alsat-1B project).

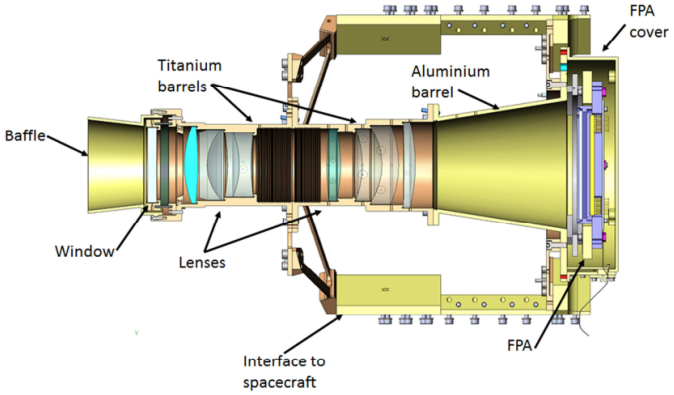

Figure 2. Cross-section of the camera assembly (ALSAT-1B project).

The lens barrel maintains the optical elements in precise geometrical alignment while ensuring thermal compensation, heat dissipation, and mechanical support. The camera structure is thermally isolated from the spacecraft by a Multiple Layer Insulation (MLI) blanket. In addition, a front window acts as both a radiation and thermal shield

to protect the front optical elements from severe thermal variations, whereas the baffle contributes to thermal equilibrium and stray-light suppression.

The payload electronics are composed of a Front-End Electronics (FEE) unit and two redundant High-Speed Data Recorders (HSDRs). The FEE contains five independent electronic cards, each dedicated to one CCD detector, enabling signal acquisition, analog-to-digital conversion, clock generation, and fault-tolerant operation. The CCD detectors are connected to the FEE through flexible printed circuit assemblies, and the processed digital data are transmitted to the HSDRs for onboard storage before downlink transmission through the X-band communication system.

2.2. Integration optical filters

The optical payload of the Alsat-1B is organized into several main subsystems, including the telescope, common optics, the focal plane assembly (FPA), and the Front-End Electronics (FEE). The FPA represents a critical element of the imaging chain and consists of the CCD detectors, the optical filter tray, and precision shims used for alignment adjustment (**Figures 3** and **4**). The assembly is based on an athermal design in which the focal plane is connected to the titanium optical barrels through an aluminium interface, allowing the optical system to maintain focus stability over the operational temperature range.

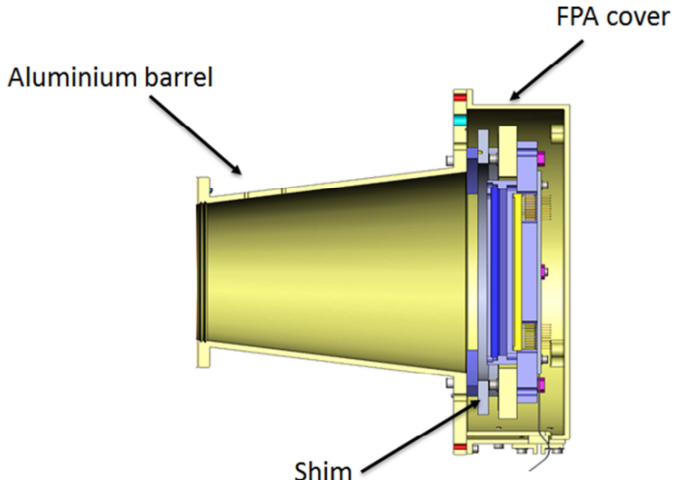

Figure 3. The focal plane in the back-aluminum barrel.

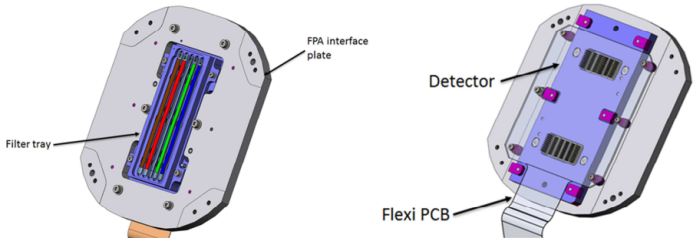

Figure 4. The focal plane assembly.

The optical filter tray is manufactured from a controlled coefficient of thermal expansion (CTE) metal–composite material specifically selected to match the thermo-mechanical properties of the ceramic CCD mounts and the surrounding metallic support structure within the FPA. This material compatibility minimizes

differential thermal deformation and preserves detector alignment under thermal cycling conditions.

The FPA integrates five spectral filters corresponding to the blue, green, red, near-infrared (NIR), and panchromatic (PAN) channels (**Figure 5**). Each filter is positioned directly above its associated linear CCD detector to selectively transmit the required wavelength band while rejecting unwanted radiation. The filters are designed as elongated strips approximately 5 mm wide and 4 mm thick and are installed inside precision-machined tilted pockets to reduce stray-light reflections and improve optical performance.

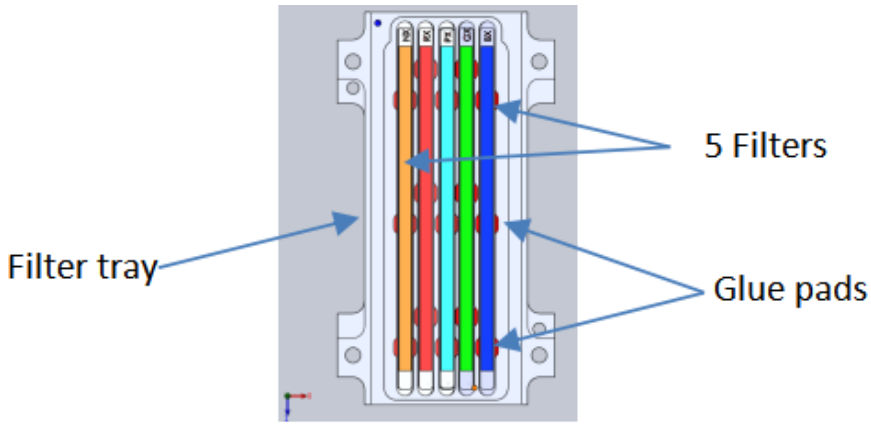

Figure 5. Filter tray assembly.

The filters are retained using a precision adhesive bonding technique based on four epoxy glue pads distributed around each filter interface. This bonding configuration ensures accurate positioning and stable mechanical fixation while limiting stress concentrations induced by launch vibration or thermal expansion mismatch. The adhesive pads also provide a compliant interface capable of absorbing small thermo-elastic deformations, thereby reducing the risk of optical distortion, filter cracking, or detector misalignment. Consequently, the bonding design of the filters is a key aspect of the payload structural and optical stability throughout launch, qualification, and orbital operating conditions.

The assembly consists of five individual optical filters corresponding to the panchromatic and multispectral spectral channels. Each filter is mounted within a dedicated cavity of the filter tray and bonded using epoxy adhesive pads strategically distributed around the filter perimeter. The adhesive pads provide both mechanical retention and stress accommodation between the optical substrate and the metallic support structure. Their dimensions, location, and number were selected to achieve a compromise between structural stiffness, thermal stress reduction, and optical stability.

The distribution of the glue pads (**Figure 6**) plays a critical role in the overall thermo-mechanical behavior of the assembly. Rather than using a continuous adhesive layer, discrete adhesive pads were employed to reduce the transfer of thermally induced stresses resulting from the mismatch between the coefficients of thermal expansion of the filter substrate and the filter tray material. This bonding strategy allows the adhesive to partially absorb differential thermal displacements while maintaining adequate structural support and alignment accuracy.

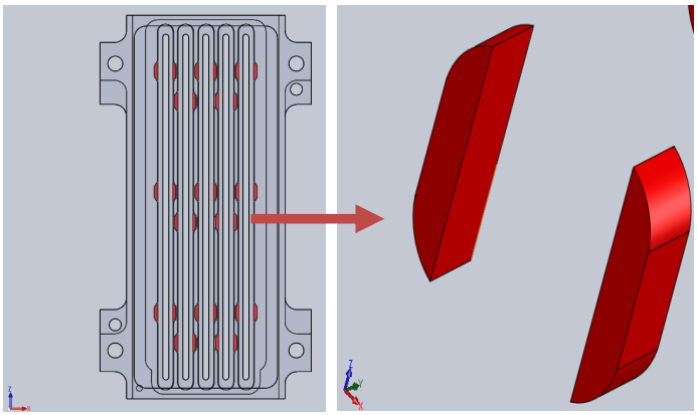

Figure 6. Distribution glue pads on filter tray assembly.

Several glue-pad configurations were investigated to evaluate their influence on stress distribution and deformation levels. The results indicate that increasing the number of adhesive contact points improves the load-sharing mechanism between the filter and the tray. A greater number of bonding points distributes thermo-mechanical loads more uniformly over the filter perimeter, reducing local stress concentrations and minimizing deformation of the optical surface. This effect is particularly important under cryogenic conditions, where thermal contraction differences become significant.

The selected filter tray configuration incorporates multiple adhesive pads symmetrically distributed around each optical filter to ensure balanced constraint conditions. The symmetric arrangement minimizes the risk of differential deformation, filter tilting, and stress localization that could negatively affect optical performance. Furthermore, the spacing between adhesive pads was optimized to provide sufficient flexibility for thermal accommodation while maintaining the mechanical integrity of the assembly during launch vibration and operational temperature cycles.

From a structural perspective, the filter tray provides a rigid support frame capable of transferring loads efficiently to the focal plane assembly. At the same time, the adhesive pads act as compliant interfaces that mitigate thermal stresses generated at the bonded joints. This combined design approach enables the assembly to maintain optical alignment and dimensional stability over a wide temperature range while reducing the risk of adhesive failure, substrate cracking, or excessive filter deformation.

3. Mechanical stress in optical filters

For detailed design, a full mechanical and structural analysis was performed in SolidWorks software. The finite element (FE) analysis of the filter assembly was performed using ANSYS 20. The material properties adopted in the simulations are summarized in **Table 1**.

Table 1. Parameters defining the materials.

Part	Filter tray	Glue	Filter
Material	CE11	Epoxy	BK 7
Young's Modulus E(MPa)	1.09×10^5	(4,700 ÷ 70) for (−40 °C ÷ 20 °C) [11]	82,000
Poisson's Ratio ν	0.26	0.39	0.21

Table 1. *Cont.*

Part	Filter tray	Glue	Filter
Coefficient of Thermal Expansion CTE $\times 10^{-6}$(K)	11	102	8
Mass Density ρ (kg/m^3)	2,500	1,260	2,520

The FE mesh model of the optical filter assembly was generated using the default meshing configuration for all components (**Figure 7**) except the adhesive glue pads, as illustrated in **Figure 8**. To accurately evaluate the mechanical stresses within the adhesive regions, a local mesh refinement strategy was specifically applied to the glue pads, since these areas exhibit high stress gradients caused by material discontinuity and adhesive bonding effects. Linear quadrilateral and quadratic quadrilateral elements were employed in these critical zones to improve stress distribution accuracy and capture local stress concentrations generated by thermal loading and differential material expansion. The remaining components were meshed using an optimized default mesh, which was considered sufficient because the stress distribution in these regions is smoother and less sensitive to mesh density.

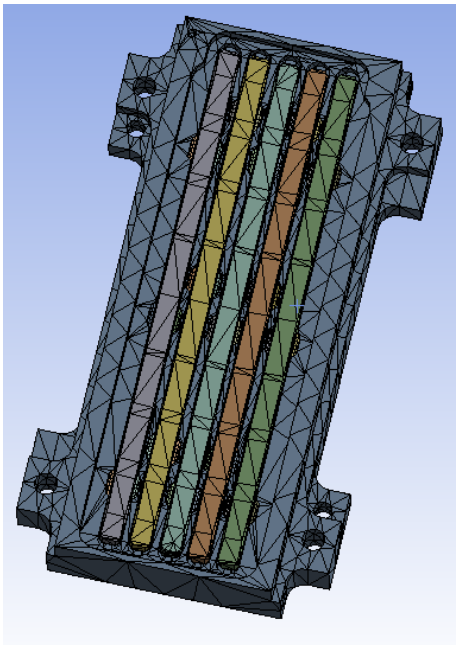

Figure 7. Default mesh for assembly monitoring.

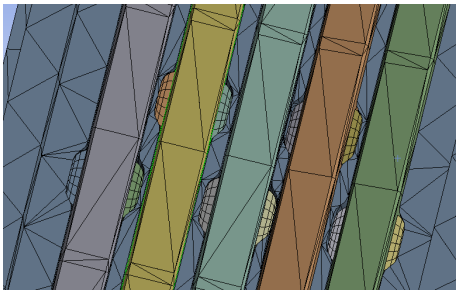

Figure 8. Refined mesh for glue pad.

The boundary conditions applied to the finite element models. The base of the main housing support is fully constrained, with all six degrees of freedom (DOF) fixed.

For solid elements, the active DOF correspond to translational displacements along the X, Y, and Z directions.

The assembly was analyzed under the following loading conditions:

- Reference ambient temperature: T = +20 °C, considered as the stress-free condition.
- Thermal loading: The structure was subjected to temperature variations ranging from 20 °C to −173 °C, with intermediate steps of approximately −10 °C, as shown in **Figure 9**. This temperature variation was selected to evaluate the thermo-mechanical behavior and structural robustness of the optical filters under a conservative cryogenic scenario representing extreme cooling conditions.
- Inertial loading: A static inertial acceleration of 1 g was successively applied along the X, Y, and Z directions.
- The lower boundary of the flexure supports was fully fixed in all directions.

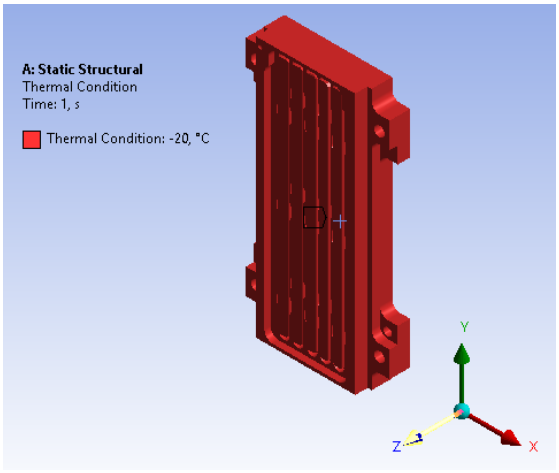

Figure 9. Thermal load distribution at 20 °C for assembly monitoring.

4. Results and discussion

Several simulation cases were conducted in this section using complementary analysis approaches to investigate the thermo-mechanical behavior of the optical filters. The study focuses on the evaluation of thermo-elastic stresses, Margin of Safety (MOS), and axial deformation under thermal and inertial loading conditions representative of launch and qualification environments.

4.1. Thermo-elastic analysis

Thermo-elastic stress analyses were conducted to evaluate the stresses induced in the adhesive pads, filters and assembly tray under thermal loading conditions. These thermal loads arise from differential expansion within the assembly, governed by the mismatch in coefficients of thermal expansion (CTE) between bonded materials when subjected to temperature variations relative to the stress-free state.

The results highlight that temperature decreases generate increasing levels of internal stress due to constrained contraction, particularly at the adhesive interfaces where material incompatibilities are most pronounced. This effect is critical in optomechanical assemblies, where even small CTE mismatches can lead to significant stress concentrations.

The analysis was performed for sixteen representative temperature cases: 20 ℃, 0 ℃, −10 ℃, −20 ℃, −30 ℃, −40 ℃, −50 ℃, −60 ℃, −70 ℃, −80 ℃, −90 ℃, −100 ℃, −120 ℃, −140 ℃, −160 ℃, and −173 ℃ covering the full range of non-operational testing conditions. **Table 2** gives the thermo-elastic maximum stresses for each element 'filter tray assembly' in MPa for different temperatures.

Table 2. Thermo-elastic stresses for each elements filter tray for different temperatures.

Temperature (℃)	Thermo-elastic stress (MPa)		
	Glue pads	Filters	Assembly tray
20	0	0	0
0	5.268	12.165	53.765
−10	10.889	18.343	80.614
−20	11.110	23.00	107.45
−30	24.436	28.834	134.26
−40	35.990	37.169	161.07
−50	41.988	43.364	187.91
−60	47.986	49.559	214.76
−70	53.985	52.041	241.60
−80	59.983	61.949	268.45
−90	65.981	68.144	295.29
−100	71.980	74.339	322.14
−120	83.976	80.952	375.83
−140	95.973	99.118	429.52
−160	107.97	111.51	483.20
−173	115.77	111.60	518.10

From **Table 2** and **Figures 10–12**, we can conclude that the thermo-elastic results show a clear and physically consistent trend: stresses increase as temperature decreases, due to constrained thermal contraction and mismatch in CTE between the bonded components.

At the temperature (20 ℃), all stresses are zero, confirming that this state is taken as the stress-free configuration. As the temperature drops, thermo-elastic develop and translate into internal stresses, particularly at interfaces.

1. Assembly tray: The tray exhibits the highest stress levels across all conditions, rising from ~54 MPa at 0 ℃ to 518 MPa at −173 ℃. This dominant response indicates that the tray likely has the largest stiffness and/or CTE mismatch relative to the assembly. It is therefore the primary driver of thermo-elastic loading and a potential risk area for structural integrity or deformation.
2. Filter: The filter shows moderate stress levels, increasing steadily with decreasing temperature (from ~12 MPa at 0 ℃ to ~112 MPa at −173 ℃). This suggests a partial compatibility with adjacent materials but still significant constraint effects.
3. Glue pads: The adhesive experiences the lowest stresses overall, but the increase remains significant (from ~5 MPa at 0 ℃ to ~116 MPa at −173 ℃). Given that adhesives typically have lower strength compared to metallic parts, this trend is important; even moderate stress levels may become critical for failure modes such as debonding or shear rupture.

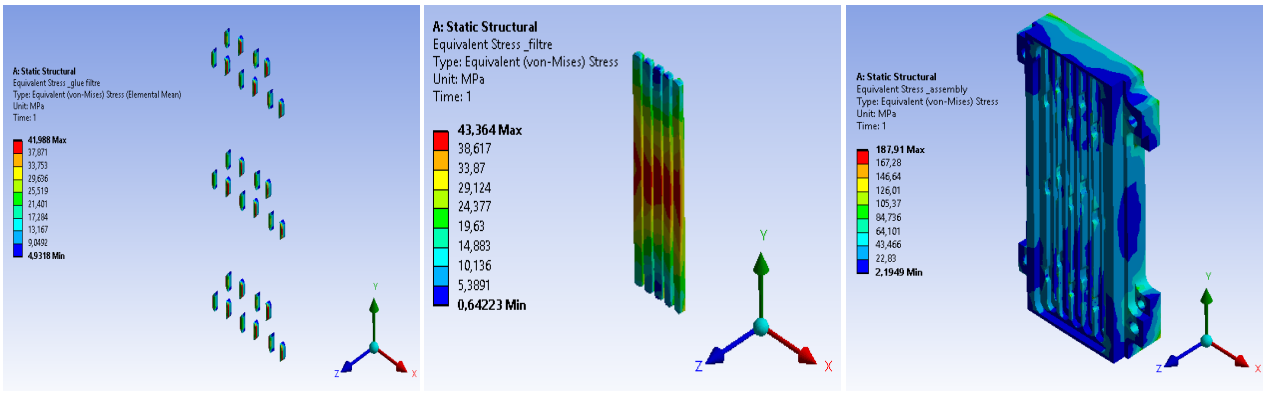

(a) **(b)** **(c)**

Figure 10. Equivalent Von-Mises stress distribution at −50 °C: **(a)** Glue pads; **(b)** Optical filters; **(c)** Assembly tray.

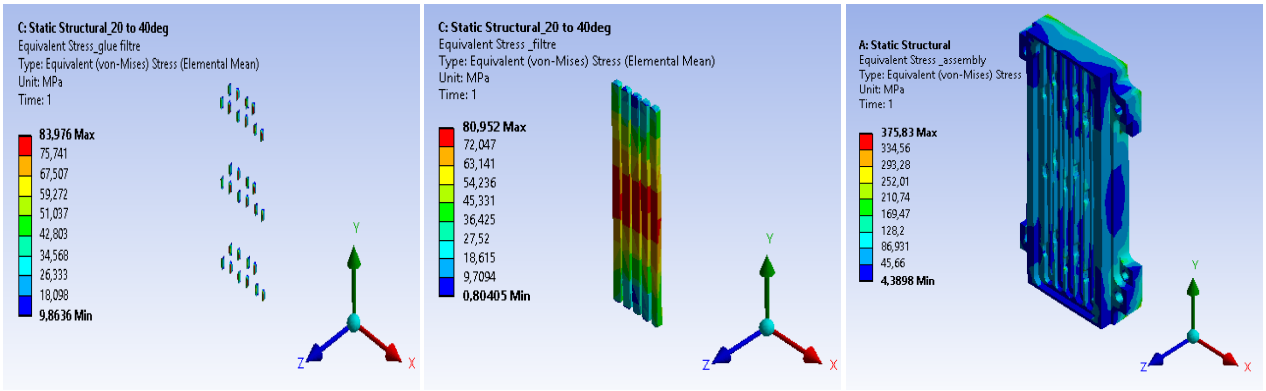

(a) **(b)** **(c)**

Figure 11. Equivalent Von-Mises stress distribution at −120 °C: **(a)** Glue pads; **(b)** Optical filters; **(c)** Assembly tray.

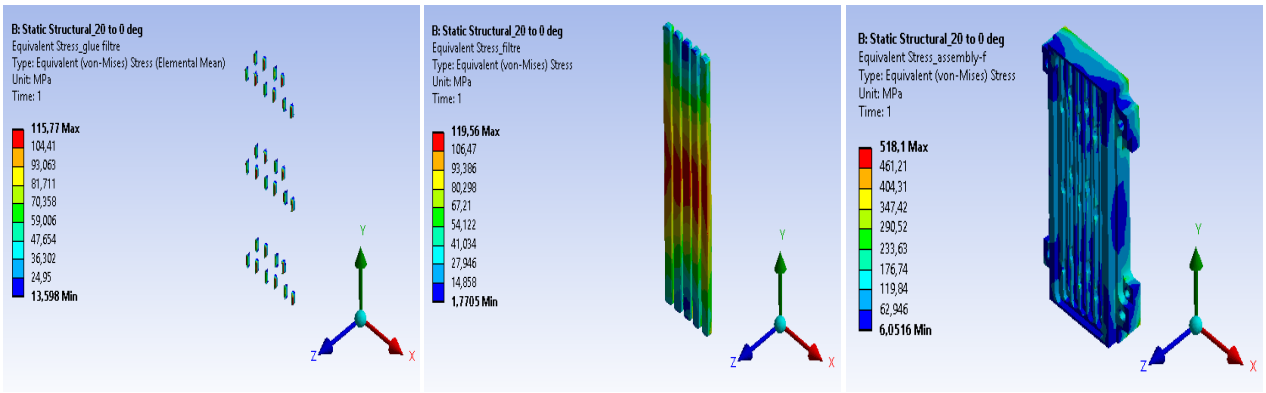

(a) **(b)** **(c)**

Figure 12. Equivalent Von-Mises stress distribution at −173 °C: **(a)** Glue pads; **(b)** Optical filters; **(c)** Assembly tray.

4.2. Margin of safety

The margin of safety (MOS) is an indicator of structural reliability that quantifies the available reserve capacity before failure occurs. It compares the allowable stress or load of a material to the actual stress or load experienced under service conditions. A positive margin indicates that the structure operates within safe limits, whereas a zero

or negative value signifies that the allowable threshold has been reached or exceeded. In practice, higher margins correspond to increased robustness and improved tolerance to uncertainties such as material variability, modeling assumptions, and environmental effects.

The safety margin is a relative measure of the material's allowable capability to the maximum working condition, as specified by the procuring activity [20–25]. The basic equation defining margin of safety for uniaxial stress is:

$$\text{MOS} = \left[\frac{\text{Allowable load}}{\text{FOS} \times \text{working load}}\right] - 1. \tag{1}$$

For uniaxial stress, the margin of safety is established by comparing the allowable stress to the applied stress, ensuring that the material can withstand the imposed loads while maintaining an adequate safety margin against failure.

In the case of the optomechanical assembly, the adhesive 3M Scotch-Weld is assigned a Factor of Safety (FOS) of 2, resulting in an allowable stress of 9 MPa. Quasi-static loading conditions representative of the launch environment are considered, with acceleration levels of 8 g in the axial direction (Z-axis) and 5 g in the lateral directions (X and Y axes). The working load is defined as three times the equivalent Von Mises stress multiplied by the corresponding directional inertial load. Based on these assumptions, the calculated MOS values for the different loading cases and spatial directions are presented in **Table 3**.

Table 3. The values of the MOS in three directions at ambient temperature.

Cases	Margin of safety		
	Z direction	**Y direction**	**X direction**
Filter_glue_assembly	1.7455	0.727	0.447

The margin of safety (MOS) values indicate that the adhesive joint in the filter assembly remains structurally safe in all three directions, since all margins are positive. However, the level of robustness varies significantly depending on the loading direction.

1. In the Z direction (MOS = 1.745), the structure exhibits a high safety margin, meaning that the allowable load is substantially greater than the applied load. This suggests strong resistance to axial loads and comfortable design margin for launch conditions.
2. In the Y direction (MOS = 0.727), the safety margin is moderate. The structure still operates within acceptable limits, but the reserve capacity is reduced compared to the Z direction. This indicates a more sensitive behaviour under lateral loading.
3. In the X direction (MOS = 0.447), the margin is the lowest, although still positive. This represents the most critical case, where the structure is closest to its allowable limit. While it remains safe, this direction may govern the design and could require attention if additional uncertainties, higher loads, or degradation effects are expected.

Overall, the assembly meets safety requirements in all directions, but the X direction is the limiting case and should be considered the driving condition for design validation and potential optimization

4.3. Filters deformation analysis

Deformation along the Y-axis corresponds to the axial displacement of the assembly under mechanical and/or thermal loading. In the case of thermo-elastic effects, this deformation is primarily driven by the expansion or contraction of materials according to their coefficient of thermal expansion (CTE). As temperature decreases, the components contract unevenly, generating relative displacements along the Y direction. When the assembly is constrained (e.g., by adhesive bonding or mechanical fixation), these free deformations are partially restricted, leading to internal stresses and displacement gradients through the thickness. Although the absolute magnitude of axial deformation is generally small, it is critical in optical systems due to their high sensitivity to misalignment [26–28].

The filter exhibits an intermediate behaviour between rigid components (such as the supporting structure) and more compliant elements (such as the adhesive). Under thermal loading, it undergoes axial deformation driven by its own CTE as well as by constraints imposed by adjacent components. This interaction can lead to differential deformation, potentially causing bending or distortion of the filter.

From an analytical perspective, the axial deformation of the filter can be estimated using the classical thermo-elastic relation:

$$\Delta Y = \alpha \cdot \Delta T \cdot L, \tag{2}$$

where α is the coefficient of thermal expansion, ΔT is the temperature variation, and L is the characteristic length along the Y-axis. However, in a bonded assembly, this free deformation is partially constrained, resulting in internal stresses. For an optical filter, this may lead to:

- Axial displacement (defocus),
- Surface deformation (optical quality degradation),
- Increased stress at adhesive interfaces.

Thus, even small deformations can have significant functional consequences. The analysis indicates that the filter behaviour strongly depends on the balance between its stiffness, the stiffness of the supporting structure, and the ability of the adhesive to accommodate differential deformation, as shown in **Table 4**.

Table 4. Deformation directional (Y-axis) optical filters for different temperatures.

Temperature (°C)	Deformation optical filters (mm)	
	Analytical	Finite element
20	0	0
0	0.0179	0.0154
−10	0.02688	0.0231
−20	0.03584	0.0307
−30	0.0448	0.0384

Table 4. *Cont.*

Temperature (°C)	Deformation optical filters (mm)	
	Analytical	Finite element
−40	0.05376	0.0461
−50	0.0627	0.0538
−60	0.0717	0.0615
−70	0.0801	0.0692
−80	0.0896	0.0768
−90	0.0986	0.0846
−100	0.1075	0.0922
−120	0.1254	0.1076
−140	0.1433	0.1230
−160	0.1613	0.1384
−173	0.1723	0.1484

The results in **Figure 13** show a clear and consistent thermo-elastic behaviour of the optical filter in the Y direction, with good agreement between the analytical prediction and the finite element results. The axial deformation increases progressively as the temperature decreases. This is expected, since the deformation is directly proportional to the temperature variation (ΔT). The evolution is almost linear over the entire range, which confirms that the filter remains within the elastic regime and that no nonlinear effects (e.g., plasticity or damage) are involved.

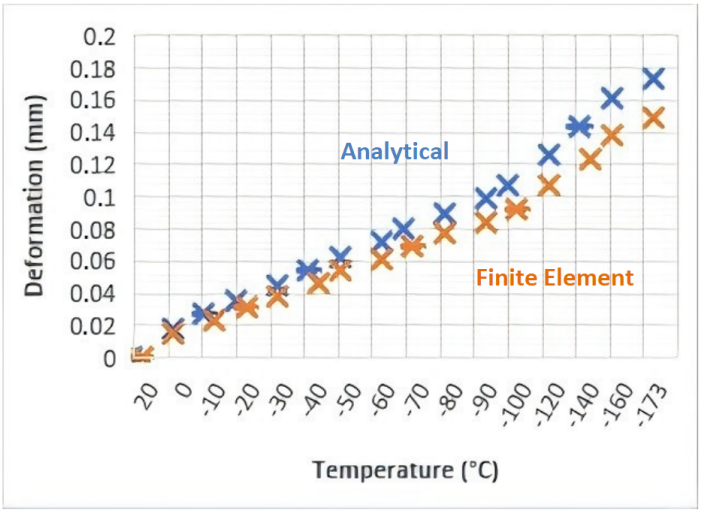

Figure 13. Axial deformation curve as a function of temperature.

For all temperature cases, the analytical values are slightly higher than the FEM results. This difference remains relatively small and consistent, indicating good correlation between both approaches. The analytical model slightly overestimates deformation because it assumes free thermal expansion, while the FEM model accounts for mechanical constraints imposed by the assembly (e.g., adhesive bonding and support stiffness), which limit the actual displacement.

The difference between the analytical and FEM results increases as the temperature decreases. For example:

- At 0 °C: difference ≈ 0.0025;

- At −100 °C: difference ≈ 0.015;
- At −173 °C: difference ≈ 0.024.

This trend indicates that the effect of structural constraints becomes more significant at lower temperatures, as the thermal mismatch between the assembly materials generates higher internal stresses that partially restrict the free deformation of the optical filter.

- The analytical solution represents the ideal behavior of the filter under unconstrained conditions.
- The FEM results represent the actual behavior of the filter within the assembly, where deformation is influenced by bonding interfaces, support conditions, and structural constraints.

The relatively small difference observed between the two approaches confirms that the analytical model provides a reliable first-order estimation of the thermo-mechanical response. However, the FEM results are more representative of the real operating conditions and therefore should be considered for the final design assessment and validation.

At low temperatures (below −100 °C), the increasing discrepancy between the analytical and numerical results highlights the importance of accounting for assembly constraints and thermo-mechanical coupling effects. This consideration is particularly critical for high-precision optical systems, where even small axial deformations may affect optical alignment, induce defocus, or degrade overall system performance.

5. Conclusion

This paper presents a comprehensive thermo-mechanical assessment of a bonded optical filter assembly, including thermo-elastic stress analysis, margin of safety (MOS) evaluation, and deformation analysis. The results provide consistent and complementary insights into the structural and functional behavior of the system under thermal and inertial loading conditions representative of space environments.

The thermo-elastic analysis revealed a clear and physically consistent trend: stresses increase significantly as temperature decreases due to constrained thermal contraction and mismatch in coefficients of thermal expansion (CTE) between the different components. While the stress-free state is confirmed at 20 °C, progressively lower temperatures generate increasing internal stresses, particularly at material interfaces. Among the components, the assembly tray exhibits the highest stress levels, identifying it as the primary driver of thermo-elastic loading and a potential critical element for structural integrity. The optical filter shows moderate stress levels, reflecting partial thermo-mechanical compatibility, whereas the adhesive glue pads, despite experiencing lower stresses, remain critical due to their comparatively lower strength and susceptibility to failure modes such as debonding or shear.

The margin of safety analysis confirms that the adhesive joints satisfy structural requirements in all loading directions, as all MOS values remain positive. However, the safety margins are direction-dependent. The Z direction presents a high margin, indicating robust resistance to axial loads, while the Y direction shows moderate

performance. The X direction constitutes the most critical case, with the lowest margin, and therefore governs the design. This highlights the need to consider lateral loading conditions carefully, especially in the presence of uncertainties or potential degradation effects over the mission lifetime.

The deformation analysis of the optical filter demonstrates a linear increase in axial displacement with decreasing temperature, confirming elastic behavior over the studied range. A good agreement between analytical and finite element (FE) results was observed, validating the analytical approach as an effective first-order estimation tool. The slight overestimation by the analytical model is attributed to its assumption of free thermal expansion, whereas the FE model accounts for assembly constraints. The increasing discrepancy at lower temperatures emphasizes the growing influence of thermo-mechanical coupling and structural constraints.

Overall, the combined analyses demonstrate that the bonded filter assembly design is structurally sound and performs within acceptable limits under the considered conditions. Nevertheless, critical aspects such as adhesive behavior, lateral loading (X direction), and low-temperature conditions (below −100 °C) require particular attention. These findings underline the importance of integrated thermo-mechanical modeling for ensuring both structural integrity and optical performance in high-precision spaceborne systems.

Funding: The research has received no external funding.

Institutional review board statement: Not applicable.

Informed consent statement: Not applicable.

Data availability statement: The data is unavailable due to privacy restrictions.

Acknowledgement: The author would like to thank the Algerian Space Agency and the Centre of Satellites Development.

Conflict of interest: The author declares no conflict of interest.

AI use statement: The author declares that no artificial intelligence (AI) tools were used in the preparation of this manuscript.

References

1. Macleod HA. Thin-Film Optical Filters, 5th ed. CRC Press; 2017. doi: 10.1201/b21960
2. Hazra L. Foundations of Optical System Analysis and Design, 1st ed. CRC Press; 2022. doi: 10.1201/9780429154812
3. Madsen CK, Zhao JH. Optical Filter Design and Analysis: A Signal Processing Approach, 1st ed. Wiley; 1999. doi: 10.1002/0471213756
4. Eccleston P, Caldwell A, Bishop G, et al. The Ariel payload design post-PDR. In: Proceedings of the Space Telescopes and Instrumentation 2024: Optical, Infrared, and Millimeter Wave; 16–22 June 2024; Yokohama, Japan. p. 48. doi: 10.1117/12.3019713
5. Willey RR. Field Guide to Optical Thin Film. SPIE; 2022. Available online: https://lab.semi.ac.cn/library/upload/files/2022/3/25101825431.pdf
6. Parkinson JC. Stress Analysis in Optical Systems [Master's Thesis]. The University of Arizona; 2023. Available online: https://wp.optics.arizona.edu/alumni/wp-content/uploads/sites/113/2024/03/Stress_Analysis_in_Optical_Systems.pdf

7. Babeva T. Special Issue: "Optical Thin Films and Structures: Design and Advanced Applications." Coatings. 2020; 10(11): 1140. doi: 10.3390/coatings10111140
8. Xiong J, Zhang Z, Jin X, et al. Theoretical modeling and calculation of stress fields in precision optical lens subjected to multi-point adhesive bonding assembly. Precision Engineering. 2022; 73: 257–269. doi: 10.1016/j.precisioneng.2021.09.008
9. Liu X, Jiao J, Gu K, et al. Design and Analysis of Optical–Mechanical–Thermal Systems for a High-Resolution Space Camera. Sensors. 2025; 25(24): 7617. doi: 10.3390/s25247617
10. Strauss GN, Pulker HK. Mechanical Stress in Optical Coatings. PhysTech Coating Technology GmbH; 2005. Available online: http://www.ptcoating.com/pdf/PhysTech-2005-7-stress%20in%20optical%20coatings.pdf
11. Maamar F, Boudjemai A. Optomechanical optimal design configuration and analysis of glue pad bonds in lens mounting for space application. Advances in Space Research. 2020; 65(10): 2263–2275. doi: 10.1016/j.asr.2020.01.025
12. Yu R, Liang R, Zhou W, et al. Stress analysis of a filter screen based on dimensional analysis and finite element analysis. Engineering Applications of Computational Fluid Mechanics. 2020; 14(1): 168–179. doi: 10.1080/19942060.2019.1665588
13. Begou T, Lemarchand F, Lemarquis F, et al. High-performance thin-film optical filters with stress compensation. Journal of the Optical Society of America A. 2019; 36(11): C113. doi: 10.1364/JOSAA.36.00C113
14. Fuis V, Kašuba D. Stress and Deformation of the Filter Press. In Proceedings of the Engineering Mechanics 2020; 24–25 November 2020; Online. pp. 146–149. doi: 10.21495/5896-3-146
15. Hale LC, Slocum AH. Optimal design techniques for kinematic couplings. Precision Engineering. 2001; 25(2): 114–127. doi: 10.1016/S0141-6359(00)00066-0
16. Su W, Zhang C, Mo D, et al. Finite element analysis of the package structure of HgCdTe infrared focal plane array detector. AIP Advances. 2024; 14(3): 035247. doi: 10.1063/5.0197564
17. Xue Y, Xu Q, Huang M, et al. Study of thermal stresses in InAs/GaSb type-II superlattice focal plane arrays via multi-scale finite element modeling. AIP Advances. 2025; 15(7): 075220. doi: 10.1063/5.0262071
18. Yoder P, Vukobratovich D. Opto-Mechanical Systems Design, 4th ed. CRC Press; 2015. doi: 10.1201/b18147
19. Keith BD, Victor LG, Gregory JM. Integrated Optomechanical Analysis, 2nd ed. SPIE; 2012.
20. Schwertz K, Burge J. Optical Effects of Mechanical Motion. In: Field Guide to Optomechanical Design and Analysis. SPIE; 2012. doi: 10.1117/3.934930.ch1
21. Vukobratovich D, Yoder P. Fundamentals of Optomechanics, 1st ed. CRC Press; 2018. doi: 10.1201/9781351210867
22. Yablon AD. Optical and Mechanical Effects of Frozen-in Stresses and Strains in Optical Fibers. IEEE Journal of Selected Topics in Quantum Electronics. 2004; 10(2): 300–311. doi: 10.1109/JSTQE.2004.826570
23. Ahmad A. Handbook of Optomechanical Engineering, 2nd ed. CRC Press; 2017. doi: 10.4324/9781315153247
24. Hatheway AE. Analysis of adhesive bonds in optics. In: Optomechanical Design. SPIE; 1993. Available online: https://wp.optics.arizona.edu/optomech/wp-content/uploads/sites/53/2016/10/Analysis-of-adhesive-bonds-in-optics-Hatheway-1993.pdf
25. Optical Society of America. Handbook of Optics: Fundamentals, Technique, and Design. McGraw-Hill; 1994.
26. Yoder PR. Opto-Mechanical Systems Design, 3rd ed. SPIE; 2005. Available online: https://spie.org/Publications/Book/659690
27. Yoder PR. Mounting Optics in Optical Instruments, 2nd ed. SPIE; 2008. doi: 10.1117/3.785236
28. Puderbach V, Kirsch R, Antonyuk S. Experimental Characterization of the Mechanical Properties of Filter Media in Solid–Liquid Filtration Processes. Materials. 2024; 17(18): 4578. doi: 10.3390/ma17184578